DOI: 10.1002/ ((please add manuscript number))
**Article type: Full Paper**

# Doped N-type Organic Field-Effect Transistors based on Faux Hawk Fullerene

*Shiyi Liu, Nicholas J. DeWeerd, Brian J. Reeves, Long K. San, Drona Dahal, Raj Kishen Radha Krishnan, Steven H. Strauss, Olga V. Boltalina, Björn Lüssem**

S. Liu, D. Dahal, R. K. R. Krishnan, Assoc. Prof. B. Lüssem
Department of Physics
Kent State University
Kent, OH, 44240
E-mail: blussem@kent.edu

N. J. DeWeerd, B. J. Reeves, Dr. L. K. San, Prof. S. H. Strauss, Dr. O. V. Boltalina
Department of Chemistry
Colorado State University
Fort Collins, CO 80523, USA.
E-mail: olga.boltalina@colostate.edu

Keywords: $C_{60}$, Faux Hawk Fullerene, Organic Field-Effect Transistor, Doping, Transfer Doping

Faux hawk fullerenes are promising candidates for high-performance organic field-effect transistors (OFETs). Faux hawk fullerenes show a dense molecular packing and high thermal stability. Furthermore, in contrast to most other $C_{60}$ derivates, functionalization of the fullerene core by the fluorinated group $C_6F_4CF_2$ does not increase their LUMO position, which allows the use of air-stable molecular n-dopants to optimize their performance. Here, the influence of n-doping on the performance of OFETs based on the faux hawk fullerene 1,9-$C_{60}$(cyclo-$CF_2$(2-$C_6F_4$)) ($C_{60}$FHF) is studied. A analytic model for n-doped transistors is presented and used to clarify the origin of the increase in the subthreshold swing usually observed in doped OFETs. It is shown that the increase in subthreshold swing can be minimized by using a bulk dopant layer at the gate dielectric/$C_{60}$FHF layer instead of a mixed host:dopant layer. Following an optimization of the OFETs, an average electron mobiliy of 0.34 $cm^2V^{-1}s^{-1}$, a subthreshold swing below 400 $mVdec^{-1}$ for doped transistors, and a

contact resistance of 10 $k\Omega cm$ is obtained, which is among the best performances for fullerene based n-type semiconductors.

## 1. Introduction

Driven by the discovery of new organic semiconductors with charge carrier mobilities in the $5-10\ cm^2V^{-1}s^{-1}$ range,[1–3] Organic Field-Effect Transistors (OFETs) have seen a significant increase in their switching speed over recent years.[4–6] In addition, the introduction of molecular contact[7,8] and channel[9–12] doping has increased their performance.[13] Doping has made organic transistors more reliable,[14,15] has opened new ways to control the threshold voltage of OFETs,[12,16,17] and has allowed for the design of new transistor concepts.[18] However, much of this progress was achieved for hole transport materials, whereas electron transport materials are still lagging behind in their performance.[19] Not only do n-type organic semiconductors have a lower charge carrier mobility, but n-doping adds further constraints on the molecular design of the dopant and the organic semiconductor. In particular, any strong decrease in the electron affinity (EA) of the organic semiconductor has to be avoided, as strong n-dopants have to be used to dope these films that tend to become unstable in ambient air.[20]

Fullerene, $C_{60}$, is the prototype of an n-type organic semiconductor.[21] Charge carrier mobilities in the range of $0.1-1\ cm^2V^{-1}s^{-1}$ are routinely achieved[22] and mobilities of up to $5\ cm^2V^{-1}s^{-1}$ were obtained in aligned crystals of $C_{60}$ grown from solution.[23] Furthermore, $C_{60}$ can be n-doped by a wide variety of dopants, including air-stable dopants that were shown to even increase the stability of spin-coated OFETs based on PCBM.[15,24] Motivated by this success, a wide variety of $C_{60}$ derivatives have been tested.[25] However, out of overall 88 $C_{60}$ derivatives summarized in a recent review by Zhang et al.,[25] only the *o*-xylene $C_{60}$ monoadduct OXCMA reported by Yu et al. shows a maximum mobility above

0.3 $cm^2V^{-1}s^{-1}$ (maximum mobility of 0.5 $cm^2V^{-1}s^{-1}$, average mobility of 0.16 $cm^2V^{-1}s^{-1}$). [26]

A recent discovery of the intramolecular $S_NAr$ annulation reaction of $C_{60}(CF_2C_6F_5)^-$ anion resulted in the synthesis of a new type of monoadduct, faux hawk fullerene, 1,9-$C_{60}$(cyclo-$CF_2$(2-$C_6F_4$)) (for brevity, $C_{60}$FHF notation is used below). In its structure shown in **Figure 1**, the fluoroorganic moiety - $C_6F_4CF_2$ - is attached via C($C_{60}$)–C(F) bonds rather than C($C_{60}$)–C(H) bonds in typical organofullerenes. The C–F bonds are stronger than C–H bonds and more polar. This chemical difference is manifested in the outstanding thermal stability of $C_{60}$FHF - it can sublime without degradation, in contrast to most $C_{60}$ organic derivatives. In fact, when $PC_{60}BM$ is subjected to high temperatures, one of the observed decomposition products is a faux hawk-like monoadduct, which is ca. 50 $kJmol^{-1}$ more stable than $PC_{60}BM$ itself.[27] This high thermal stability of $C_{60}$FHF provides added flexibility in its processing for device testing, in particular as it allows for purification of the material via sublimation and for controlled film deposition by vacuum sublimation.

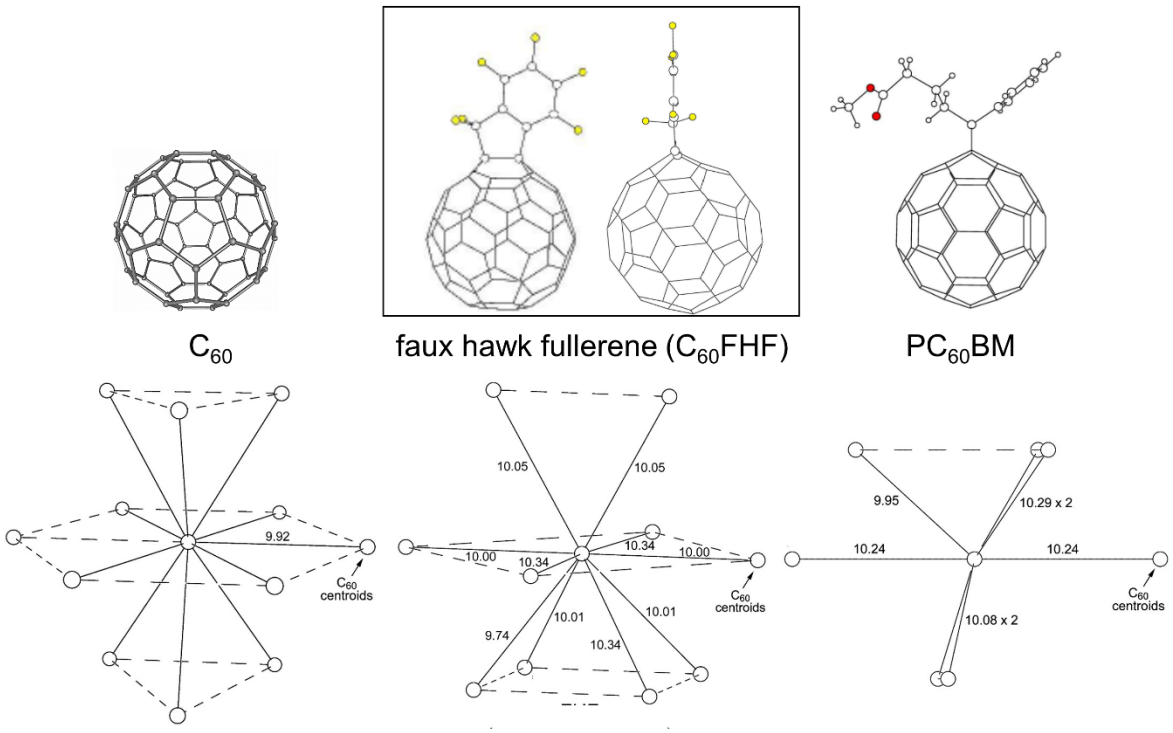

**Figure 1.** Top: Drawings of molecular structures of $C_{60}$, $C_{60}$FHF (two views) and $PC_{60}BM$. Bottom: The nearest-neighbor centroid packing patterns in the single-crystal X-ray structures of $C_{60}$ (left), [28] $C_{60}$FHF (middle), [29] and $PC_{60}BM$ (right). [30]

The compact shape of the faux hawk moiety and attractive intermolecular F…F interactions allow for a tight packing of the molecules in the solid phase as evidenced from the comparison of the packing pattern of $C_{60}$FHF[29] with those of underivatized $C_{60}$[28] and $PC_{60}BM$[30] based on the solvent-free single crystal X-ray data (Figure 1). In the case of $PC_{60}BM$, there are only seven nearest neighbor molecules with the $C_{60}$ cage centroid distances of 9.95–10.28 Å (median distance is 10.24 Å); in the case of $C_{60}$FHF, there are ten nearest neighbor molecules with the centroid-centroid distances of 9.74–10.34 Å (median distance is 10.02 Å), and in the case of underivatized $C_{60}$, there are twelve nearest neighbor molecules with the median centroid-centroid distance of 9.92 Å. As a result, the density of the crystalline $C_{60}$FHF is 16% higher than that of $PC_{60}BM$ (and it has only 1.1 % larger molar mass). This efficient packing involving cage-to-cage interactions of π-systems assisted by weak attractive F….F[31–33] interactions may enable strong intermolecular electronic coupling in the solid state, improved transport properties and higher charge carrier mobilities. Finally, $C_{60}$FHF has the same lowest unoccupied orbital (LUMO) as $C_{60}$, when estimated from the $E_{1/2}(0/-)$ values measured by cyclic voltammetry in solution.[29] Usually, reducing the π-system of $C_{60}$ by functionalization raises the LUMO energy, as observed for most organic derivatives of $C_{60}$ with hydrocarbyl groups or cycloadducts. In the faux hawk fullerene, the electron-withdrawing effect of the fluorinated group $C_6F_4CF_2$ cancels out the effect of reduction of the $C_{60}$ π-system by one double bond. Hence, in addition to the anticipated ease of injection of charge carriers from the source contact into the $C_{60}$FHF layer, it should be possible to use the same dopants as for $C_{60}$, including air stable n-dopants such as o-MeO-DMBI-I.

Thus, faux hawk fullerenes may represent a new class of n-type organic semiconductors that show potential to overcome notorious limitations of organofullerenes and to provide high charge carrier mobilities.[29]

Here, a significantly improved one-step synthesis of $C_{60}$FHF is described that allows for more efficient and larger-scale preparation and purification compared to the original report.[29] The improved synthesis allows the systematic study of the performance of $C_{60}$FHF in vacuum-processed organic field-effect transistors, in particular the influence of contact and channel doping on the performance of the transistors. By deriving an analytical solution for the drain current of an n-doped OFET operated in saturation, it is shown that the subthreshold swing of doped transistors can be optimized by using a transfer doping approach, i.e. by including a bulk dopant layer at the interface between organic semiconductor and gate dielectric instead of a mixed doped layer.

Using optimized OFETs, a charge carrier mobility of 0.35 $cm^2V^{-1}s^{-1}$ is obtained, which is among the highest performances for fullerene derivates. Furthermore, by an optimization of the gate oxide, transistors with a very small subthreshold swing ($SS = 116\ mVdec^{-1}$) are obtained, which increases slightly to $355\ mVdec^{-1}$ for highly doped transistors.

## 2. Improved Synthesis of $C_{60}$FHF

The first synthesis of $C_{60}$FHF was reported in 2015.[29] It utilizes a two-step reaction, which requires (i) synthesis and isolation of a hydrofullerene precursor by a laborious high-performance liquid chromatography (HPLC) and then (ii) a reaction of hydrofullerene with proton sponge to form the final product, $C_{60}$FHF, which is further purified by HPLC. It was also reported that $C_{60}$FHF can be synthesized in a single-step reaction, but only with a low yield of 7%. Such a situation makes it difficult to synthesize large amounts of purified $C_{60}$FHF for OFET device studies, therefore, a series of optimization experiements are carried

out aimed at improving the yield of $C_{60}FHF$, scaling up and decreasing overall time for preparation and purification.

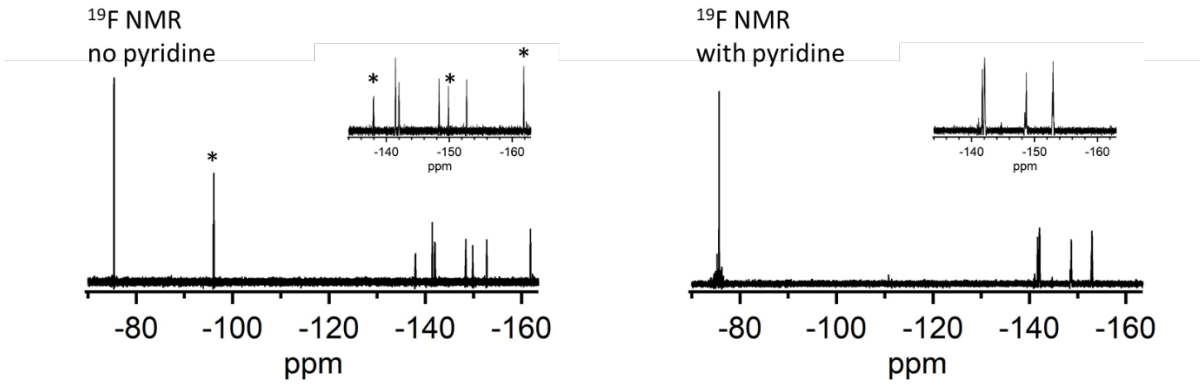


**Figure 2.** $^{19}F$ NMR spectra of crude products of two reactions performed under identical conditions, except for use of pyridine. The left panel shows the product mixture from a reaction without pyridine. The signals with asterisks are due to hydrofullerene. The right panel shows that use of pyridine results in quantitative conversion of hydrofullerene in the $C_{60}FHF$ in one step.

The most significant change to the reported procedure involves decreasing the number of reaction steps from two to one. This is achieved by introducing an organic base, pyridine, in the starting reaction mixture, which allows the process of deprotonation of the hydrofullerene to occur in situ, immediately after its formation. **Figure 2** compares $^{19}F$ NMR spectra of crude products of a two-step synthesis (left) and a one-step synthesis: note the absence of hydrofullerene in the latter product. Not only does this innovation make the second step unnecessary, but it also uses lower relative amounts of reagents, i.e., tributyl tin hydride and perfluorobenzyl iodide. For example, going from the published 10 equiv. tributyl tin hydride and 20 equiv. perfluorobenzyl iodide to 4 and 8 equiv., respectively, a single-step syntheis yields 14% $C_{60}FHF$. Other reaction parameteres varied, such as reaction time, $C_{60}$ concentration, reaction medium (replacing higher-boiling *o*-dichlorobenzene for 1-chlorobenzene) and the mode of addition of the base (dropwise or all at once), each resulting

in incremental improvements. Good reproducibility is demonstrated by performing the reaction at 250-mg scale of $C_{60}$. These studies indicated that the outcome of the reaction is strongly dependant on the presence of traces of moisture (in solvents, reagents and even glassware). Further modifications involved developing an advanced protocol for rigorous exclusion of moisture (see detail in ESI), which resulted not only to further reduction in relative amounts of reagents (going from 4 equiv. tributyl tin hydride and 8 equiv. perfluorobenzyl iodide to 1.1 equiv., for both reagents) but also in improved selectivity towards $C_{60}$FHF, which, in turn, significantly facilitated purification. Currently, 22% isolated yield of 99%-pure $C_{60}$FHF is readily achieved in a one-step synthesis and one-stage HPLC purification. The reaction is scalable, and more reagent-and solvent-economical than reported previously. For this work, 100 mg of $C_{60}$FHF is prepared, as desribed in ESI.

**3. Characterization of Organic Field-Effect Transistors**

The improved and scaled up synthesis described above allows for the testing of $C_{60}$FHF in a series of OFET devices. The general design of the OFETs studied here is shown in **Figure 3.** The parameters varied within each series and between the different series are listed in **Table 1**.

The transistors consist of an aluminium gate electrode, which is anodized to grow a thin $Al_2O_3$ layer on its surface (50 nm in series #1 and #2, 5 nm in series #3). To increase the stability of the transistors, the oxide layer is covered either by a thin layer of tetratetracontance (TTC, series #1 and #2)[34] or by a self-assembled monolayer of phosphonic acid (series #3).[35] At the interface between the transistor channel consisting of $C_{60}$FHF and the gate oxide, a thin layer (thickness of $0, 1, 2, 4$ Å) of the n-dopant o-MeO-DMBi-I[15] is deposited by vacuum deposition to control the threshold voltage of the transistors.[13]

**Table 1.** Summary of OFET Devices

| OFET series | #1 | #2 | #3 |
|---|---|---|---|
| Thickness of $Al_2O_3$ gate oxide [nm] | 50 | 50 | 5 |
| Passivation Layer | TTC (40 nm) | TTC (40 nm) | SAM |
| Injection Layer | Au | n-doped $C_{60}$ | n-doped $C_{60}$ |
| Thickness of dopant layer [Å] | 0,1,2,4 | 0,1,2,4 | 0,1,2,4 |
| Channel Length [$\mu m$] | 100, 150, 200 , 250, 300, 350 | | |

Finally, in order to study the contact resistance of these devices, two different contact geometries are used, shown in Figure 3a and b. In the first contact geometry (Figure 3a, series #2 and #3), a 25nm heavily n-doped (8wt.%) layer of $C_{60}$ ($C_{60}$:o-MeO-DMBI-I) and a thin layer (2nm) of n-dopant (o-MeO-DMBI-I) is deposited as the injection layer, which is known to generate a quasi-ohmic contact to reduce the injection losses.[36] Finally, in the second series of devices, gold contacts are used (Figure 3b, series #1). In order to ensure the horizontal conductivity on electrodes, all contacts are covered by an aluminum film (60nm) on top of the source and drain.

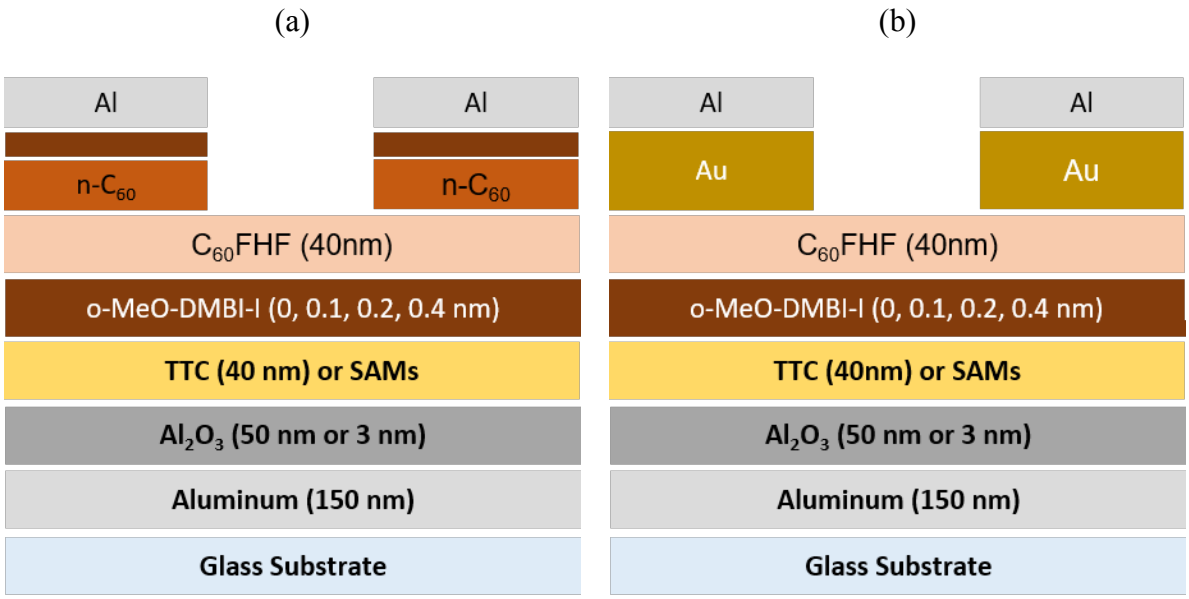


**Figure 3.** Design of OFETs used to study the performance of faux hawk fullerene, $C_{60}$FHF. To study injection into the organic semiconductor, different source/drain contact materials

are used: an n-doped injection layer (a) and Au (b). Furthermore, a thin layer of the n-dopant o-MeO-DMBI-I is introduced between the dielectric gate and the intrinsic FHF layer to control the threshold voltage of these transistors. The gate dielectric $Al_2O_3$ is either covered by a thin layer of TTC or by a self-assembled monolayer (SAM) of a phosphonic acid.

### 3.2. Stability of FHF based OFETs

A high stability of the transistor is critical to be able to reliably extract parameters such as threshold voltage and contact resistance. A hysteresis in the transfer characteristic of OFETs is often observed and can be explained by trap states at the interface of the gate dielectric and the organic semiconductor. TTC is known to eliminate these traps on the surface of the gate oxide, which leads to a reduction in the hysteresis.[34,37] Similarly, ultra-low voltage OFETs based on gate-oxides covered by phosphonic acid SAMs[35] are known to show a small and defined gate bias stress effect.[38]

The stability of a representative OFET from series #1 (cf. Table 1), but without channel doping, is shown in **Figure 4a.** Neither does cycling the transistor alter the gate and drain current, nor is a hysteresis visible. The threshold voltage does not change considerably over the number of cycles (cf. **Figure 4b**, which plots the threshold voltage for one transistor from series #1 and for one transistor from series #2, both without channel doping) for both contact materials, i.e. for Au (black symbols) and n-doped $C_{60}$ (red symbols) contacts. Overall, the stability observed is sufficient for a detailed analysis of the influence of contact and channel doping on the transistor behavior.

(a) (b)

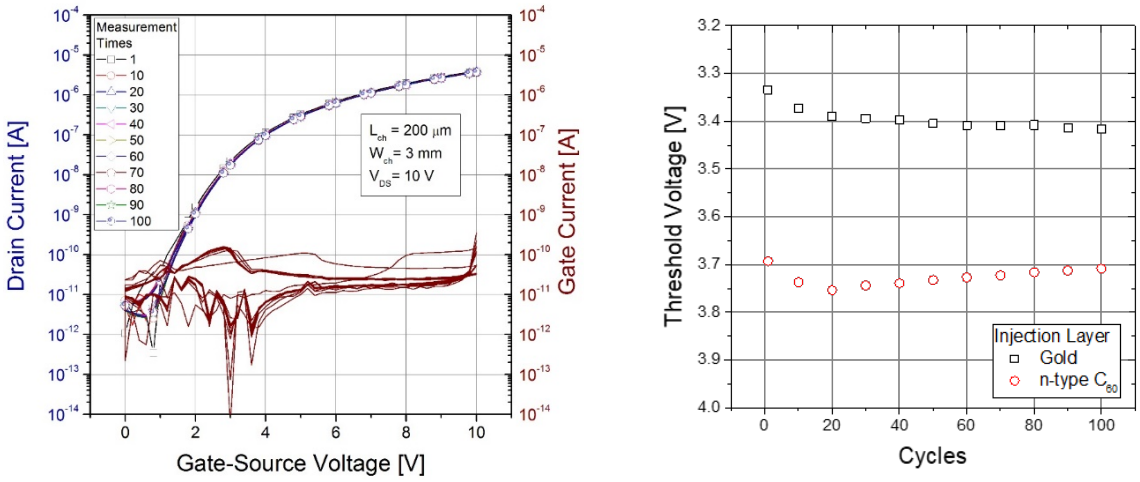


**Figure 4.** (a) Stability of OFET with device configuration #1 as shown in Table 1 (no channel doping). No significant change in the transfer characteristic is observed for 100 cyles. (b) Threshold voltage for one transistor from series #1 with Au contacts and for one transistor from series #2 with doped $C_{60}$ contacts, both without channel doping. In both geometries, the threshold voltage shown remains stable under repeated cycling.

### 3.2. Contact Doping

Any injection barrier at the source and drain electrode can significantly limit the performance of OFETs.[39] In fact, OFETs are currently not primarily limited by the relatively modest charge carrier mobility of organic semiconductors, but by the surprisingly large contact resistances encountered at common source and drain electrodes.[40] Furthermore, neglecting contact resistances and the voltage dependency of contact resistances can lead to an erroneously large charge carrier mobility extracted from the electrical characteristic of the OFETs.[3]

(a) (b)

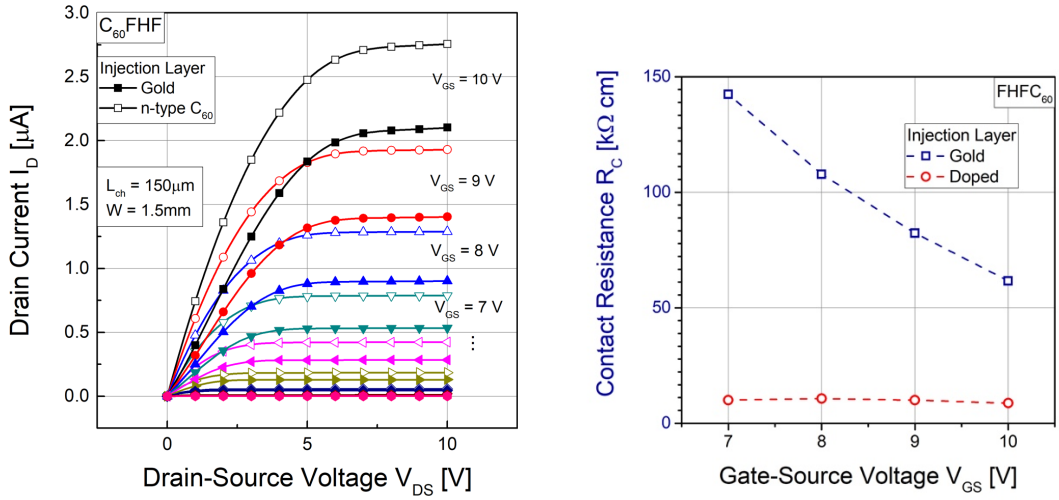


**Figure 5.** Influence of contact resistance on transistor performance. (a) shows the output characteristic of transistors with Au source and drain contacts and with source drain contacts consisting of doped $C_{60}$. (b) displays the dependence of the contact resistance on the gate source voltage.

As shown in Section 2, $C_{60}FHF$ shows an almost identical LUMO level compared to $C_{60}$, i.e. any interface barrier between $C_{60}$ and $C_{60}FHF$ should be minimal. Furthermore, a doped $C_{60}$ layer was shown to form an ohmic contact between a metallic source electrode and the organic semiconductor and to minimize the contact resistance.[7] Hence, it is expected that a doped injection layer consisting of $C_{60}$:O-MeO-DMBI-I included between a metallic source/drain electrode and the $C_{60}FHF$ channel layer as shown in Figure 3a will lead to a reduction in contact resistance Au source/drain electrodes (cf. Figure 3b).

In **Figure 5a**, the output characteristics of OFETs using a doped injection layer and OFETs using Au contacts are compared. At identical operation conditions, i.e. identical gate-source voltage $V_{GS}$ and drain-source voltage $V_{DS}$, the transistors using Au contacts show a lower drain current $I_D$. Accounting for the small difference in threshold voltage between Au and doped contacts seen in Figure 4b would even slightly increase the difference in drain current. This reduction in drain current correlates with an increased contact resistance $R_C$, plotted in

**Figure 5b.** Whereas OFETs using Au contacts show a contact resistance of 150 – 50 $k\Omega cm$, the contact resistance is reduced by the inclusion of the doped layer to 10 $k\Omega cm$. The range of contact resistances observed here is in line with other literature results studying injection into $C_{60}$ based OFETs.[41,42] Most importantly, the dependency of the contact resistance, $R_C$, on the gate-source voltage, $V_{GS}$, is greatly reduced for the OFETs with doped layers, which will make the calculation of the charge carrier mobility of the corresponding OFETs more reliable.[3]

### 3.3. Channel Doping

Doping organic transistors was shown to be effective in controlling transistor properties, in increasing their performance, and in making organic transistors more reliable.[13] For p-type transistors, it was shown that doping the transistor channel leads to a shift in the threshold voltage, $V_{th}$, according to [12,13,43]

$$V_{th} = V_{FB} + \frac{e\, d_{dop} N_A}{C_i}, \qquad \text{(Eq. 1)}$$

where $V_{FB}$ is the flatband voltage of the MIS capacitor formed between gate and source, $C_i = \frac{\epsilon_i}{d_i}$ is the capacitance per unit area of the gate, $\epsilon_i$ is the permittivity of the gate insulator, $d_i$ the thickness of the gate insulator, $e$ is the elementary charge, $d_{dop}$ is the thickness of the doped layer, and $N_A$ is the density of active dopants in the channel, which is equivalent to the density of free holes generated by doping.

For n-type transistors, though, the use of doping is less frequent and a thorough study of the impact of channel doping on the transistor performance is missing. One exception is the study of Olthof et al., who showed that n-doping can be used to fill trap states in the n-type semiconductors, which increases the charge carrier mobility and their air-stability. [15,44]

Following the same arguments as previously used to discuss the influence of channel doping of p-transistors,[16] the saturation drain current $I_{D,sat}$ of a n-doped OFET with a homogenous thickness of the doped layer of $d_{dop}$ becomes (cf. Eq. S10 of the ESI)

$$I_{D,sat} = \frac{\mu_n w C_i}{2L}\left[(V_{GS} - V_{th})^2 - \frac{2}{3}\frac{e d_{dop} N_D}{C_i} \cdot (V_{PO} - V_{th})\right] \quad \text{(Eq. 2)}$$

$$V_{th} = V_{FB} - \frac{e\, d_{dop} N_D}{C_i} \quad \text{(Eq. 3)}$$

$$V_{PO} = V_{th} - \frac{e N_D d_{dop}}{2C_s} \quad \text{(Eq. 4)}$$

where $\mu_n$ is the electron mobility inside the organic semiconductor, $V_{GS}$ is the gate-source voltage, $L$ is the channel length, $w$ the channel width, $N_D$ denotes the density of *active* dopants, $C_S = \frac{\epsilon_S}{d_{dop}}$ is the ratio of the permittivity of the doped layer $\epsilon_S$ and its thickness, and $V_{PO}$ is the so-called pinch-off voltage of the transistor.

The pinch-off voltage $V_{PO}$ describes the fact that an additional voltage has to be applied to the gate of the transistor to fully deplete the channel from the doped charges and completely turn the transistor off. It can be determined by (cf. Eq. S11 of the ESI)[45]

$$V_{PO} = V_{FB} - \frac{e N_D {d_{dop}}^2}{2\epsilon_s}\left[1 + 2\frac{d_i}{d_{dop}}\frac{\epsilon_s}{\epsilon_i}\right] \quad \text{(Eq. 5)}$$

A large pinch-off will increase the sub-threshold swing of the transistors, i.e. the transition between the on and off state is less sharp. In order to minimize this effect, the difference between the threshold and pinch-off voltage $V_{th} - V_{PO} = \frac{e N_D d_{dop}}{2C_s} = \frac{e N_D d_{dop}^2}{2\epsilon_s}$ has to be minimized. This can be accomplished by reducing the thickness of the doped layer $d_{dop}$ as much as possible, while keeping the product $N_D d_{dop}$ needed to reach a certain shift in the threshold voltage (cf. Equation 3) constant.

In the transistors discussed here (cf. Figure 3), the thickness of the doped layer $d_{dop}$ is minimized by adding a bulk layer of dopants instead of a mixed doped film on top of the dielectric gate. This doping approach, sometimes referred to as transfer or remote doping,[46–

[48] was used previously to reduce the negative impact of doping on the charge carrier mobility of the organic semiconductor.[49] In this configuration, the effective thickness of the doped layer $d_{dop}$ will mainly be determined by the Debye length in the organic semiconductor, which describes how far the charge generated at the dopant/ $C_{60}FHF$ spreads into the organic semiconductor. The Debye length was estimated to be in the range of several Angstroms in a highly p-doped layer of the hole transport material MeO-TPD.[50] As the Debye length scales with the square root of the doping concentration, a Debye length in the range of a few nanometer can be expected in the intrinsic $C_{60}FHF$ layer.

However, the effective thickness of the doped layer, $d_{dop}$, obtained by the transfer doping approach will not only depend on the Debye length, but on the roughness of the gate dielectric/organic semiconductor interface as well. If this interface is very rough, the effective interfacial area between the dopant layer and the intrinsic semiconductor will be increased, leading to a stronger doping effect and hence a larger density of dopants per unit area $N_D d_{dop}$.

(a) (b)

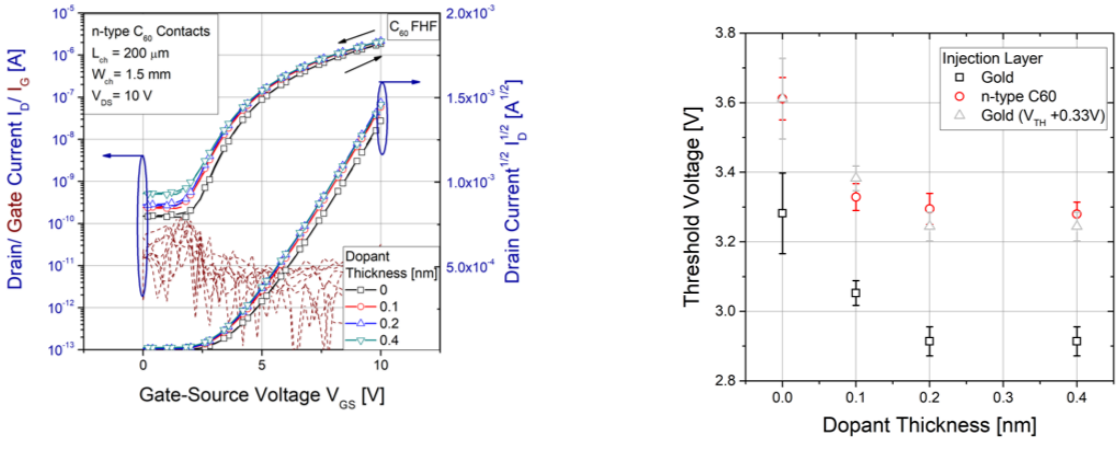


**Figure 6.** (a) Influence of channel doping on the transfer characteristic of transistors using 50 nm of $Al_2O_3$ covered with TTC as gate oxide. (b) Shift in threshold voltage with increasing dopant layer thickness for different contact geometries.

The transfer characteristics of OFETs based on a 50 nm thick $Al_2O_3$ layer covered with TTC as gate insulator (series #2) are shown in **Figure 6a**. The thickness of the o-MeO-DMBI-I dopant layer is increased from 0, 0.1, 0.2, to 0.4 nm**.** A small shift in the transfer characteristic for thicker dopant layers is visible. For a larger number of devices, this shift in threshold voltage with increasing dopant layer thickness is confirmed for devices using doped $C_{60}$ (red symbols) and Gold (black symbols) as source drain contact (cf. **Figure 6b**).

Overall, the threshold voltage shifts by approximately 0.3 V independently of the choice of the injection layer. Furthermore, the strongest shift is observed for the first two Angstroms, above which the threshold voltage saturates.

Figure 6b indicates as well that there is a constant shift between the threshold voltage obtained for Gold and for doped $C_{60}$ contacts. Indeed, if the threshold voltage obtained for Au source/drain contacts is shifted by 0.33 V, the trend of both series match well within the experimental errors (gray symbols in Figure 6b). A potential explanation for this behavior can be found in Eq. 3. Here, it is shown that the threshold voltage, $V_{th}$, depends linearly on the flatband voltage, $V_{FB}$ of the MOS capacitor. The flatband voltage in turn depends on the difference in the work function of the gate metal and the source contact, which means that a change in the contact materials (i.e. from Au to n-doped $C_{60}$ as in our experiments) is indeed expected to cause a smaller shift in threshold voltage.

Using Equation 3, a maximum density of charges per unit area introduced by doping $N^{\blacksquare} = d_{dop} N_D$ can be estimated to be in the range of $9 \cdot 10^{10}\ cm^{-2}$ ($\Delta V_{th} = 0.3\ V; C_i = 49.8\ nF cm^{-2}$). This density is rather small and, combined with the small effective thickness of the doped layer $d_{dop}$, does not increase the subthreshold swing significantly.

To study the doping effect further, the results shown in Figure 6 obtained for transistors using a thin TTC layer on top of the gate dielectric are compared to results obtained for transistors

with a much thinner $Al_2O_3$ layer, which is coated with a thin phosphonic acid SAM (series #3, cf. Table 1). The results are shown in **Figure 7**.

(a) (b)

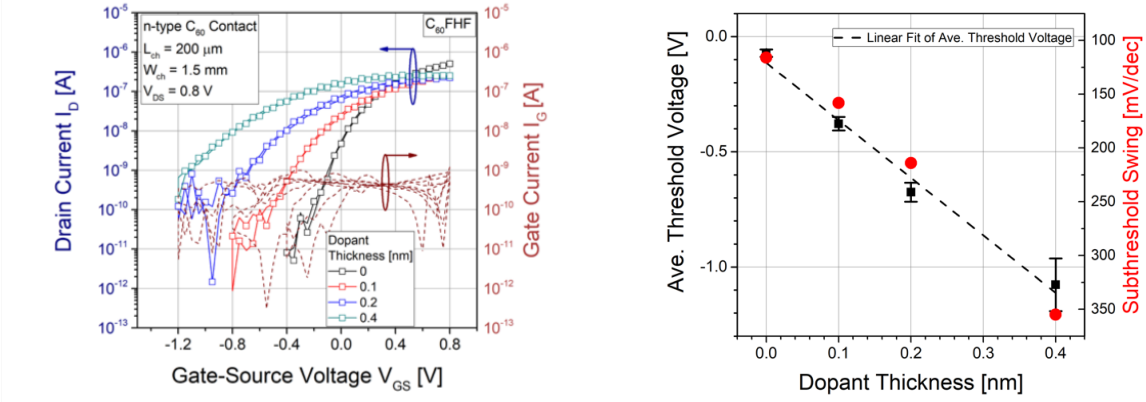


**Figure 7.** (a) By reducing the thickness of the gate oxide to 5nm and replacing TTC with a phosphonic-acid based SAM (series #3, cf. Table 1), the operation voltage of $C_{60}$FHF based transistors can be reduced to below 1 V. (b) The threshold voltage and the subthreshold swing of doped $C_{60}$FHF transistors depends on the thickness of the dopant layer.

**Figure 7a** shows that the effect of doping is much stronger in these low-voltage transistors. Overall, the threshold voltage shifts by approximately 1 V (cf. **Figure 7b**) between the undoped transistor and the transistor with a dopant layer thickness of 0.4 nm. This corresponds to a density of charges introduced into the channel per unit area $N^{\blacksquare} = N_D d_{dop} = 3.8 \times 10^{12}\ cm^{-2}$ ($\Delta V_{th} = 1\ V; C_i = 606.6\ nF cm^{-2}$), which is 1–2 orders of magnitude larger compared to the transistors based on TTC shown in Figure 6. Furthermore, the shift in threshold voltage does not seem to saturate as for the TTC transistors. Corresponding to this larger density of doped charges, the subthreshold swing is increased from approx. 116 $mV dec^{-1}$ for the undoped transistor to 355 $mV dec^{-1}$ for the transistor with 0.4 nm thick dopant layer (cf. **Figure 7**b). Still, the transistors operate at voltages below $\pm 1.2\ V$, which is on par with best OFETs reported in literature.

The precise origin of the stronger doping effect in the SAM based OFETs is currently unknown. However, as discussed above, the efficiency of the transfer doping approach will strongly depend on the morphology of the dopant layer and, additionally, the morphology of the interface between the dopant layer and $C_{60}$FHF. Any increased roughness at this interface will result in an increased interaction between dopant and $C_{60}$FHF and therefore a larger doping effect and stronger shift in threshold voltage.

### 3.4. Electron Mobility

The compact shape of faux hawk fullerenes and their tight packing should facilitate strong electronic coupling between π-systems, which is expected to result in a high charge carrier mobility. Furthermore, the transfer doping approach used here to control the threshold voltage in the transistor channel is expected to not negatively impact the charge carrier mobility as otherwise observed in mixed host/dopant layers.[49]

The charge carrier mobility for $C_{60}$FHF based OFETs is plotted vs. the thickness of the dopant layer in **Figure 8**. For TTC based OFETs (**Figure 8a**, series #1 and #2) an average charge carrier mobility in the range of $0.34\ cm^2V^{-1}s^{-1}$ is reached. The charge carrier mobility is independent of the dopant layer thickness for transistors using doped injection contacts (black symbols), but slightly decreases when the thickness of dopant film is thicker than 0.2 nm. On the contrary, when gold is used as injection layer, charge mobility increases from $0.26\ cm^2V^{-1}s^{-1}$ to $0.33\ cm^2V^{-1}s^{-1}$ for thicker dopant layers. The slightly lower charge carrier mobility for OFETs with gold source/drain contacts for thinner dopant layers (below 0.2 nm) can be explained by the contact limitation of these transistors already seen in **Figure 5**. However, when dopant layer thickness exceeds 0.2 nm, OFETs with gold as injection layer achieve a similar charge mobility as OFETs using n-type $C_{60}$ at the source/drain contacts. Considering that a thicker dopant film introduces more free charge carries into the channel, it

seems that a sufficiently large charge carrier density improves the injection of charge carriers as well, leading to a reduction of the contact limitation.[51]

The trends for SAM based OFETs having a much thinner gate dielectric shown in **Figure 8b** (series #3) are surprisingly different to TTC based devices**.** Here, The charge mobility drops from 0.15 $cm^2V^{-1}s^{-1}$ to 0.04 $cm^2V^{-1}s^{-1}$ already for a dopant layer thickness of 0.1 nm and to 0.02 $cm^2V^{-1}s^{-1}$ for thicker dopant layers. This observation is in line with the increased density of charges introduced per unit area $N^{\blacksquare} = N_D d_{dop} = 3.8 \times 10^{12}\ cm^{-2}$ mentioned in the discussion above, which was rationalized by an increased roughness at the dielectric/transistor channel interface. Whereas the increased roughness maximizes the interaction of the dopant layer with the transistor channel, i.e. more charges are generated, the increased roughness would decrease the charge carrier mobility as well. However, the precise origin of the reduced mobility observed in SAM based OFETs is currently unknown, and additional factors, such as a larger grain size of $C_{60}$FHF crystallites grown in TTC are likely to play a role as well.

(a) (b)

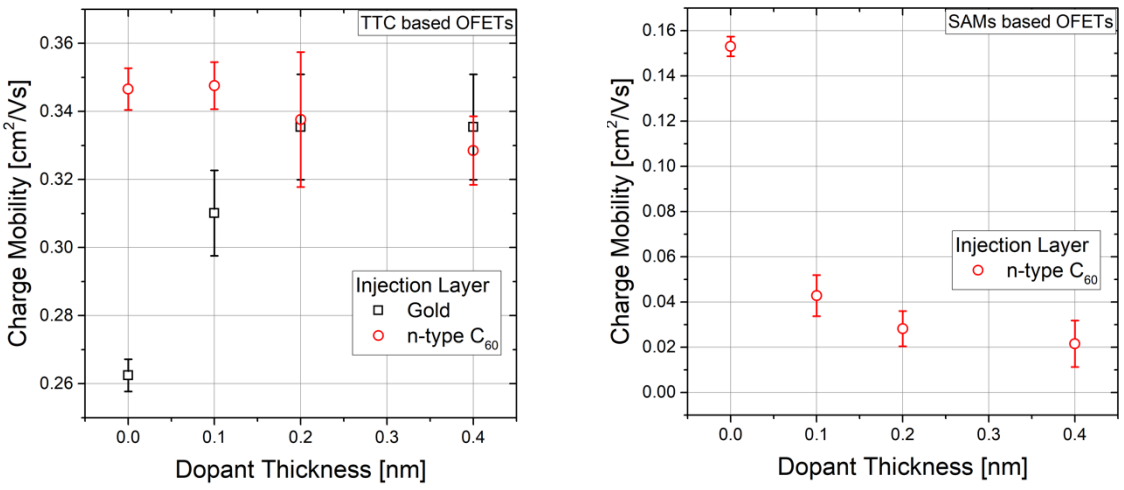

**Figure 8:** Influence of channel doping on the charge carrier mobility of $C_{60}$FHF: (a) TTC based OFETs (series #1 and #2, each data point contains result from 8 devices); (b) OFETs based on a much thinner gate dielectric covered with a phosphonic acid SAM (series #3, where each data point contains result from 4 devices).

Overall, the charge carrier mobility observed here is larger than the mobility of all other fullerene derivates discussed in literature so far,[25] in particular if only materials are compared that can be purified and deposited by sublimation.

## 4. Conclusion

Faux hawk fullerenes are promising candidates for high-performance n-type organic field-effect transistors. In particular the faux hawk fullerene discussed here 2,9-$C_{60}$(*cyclo*-$CF_2$(2-$C_6F_4$)) ($C_{60}$FHF) combines high thermal stability, good charge transport properties, with favorable LUMO energies that allow for stable n-type doping.

Doping can be used to optimize transistor performance in several ways. Contact doping is used to minimize source/drain contact resistances. Furthermore, a bulk film of dopants is added between the gate dielectric and the organic semiconductor, which dopes the channel region and shifts the threshold voltage of the transistors.

With the help of an analytic solution for the drain current of n-doped OFETs in saturation, the influence of doping on the subthreshold swing is discussed. It is shown that any increase in subthreshold swing is reduced by a reduction in the thickness of the doped layer, whereas the density of dopants per device area can be kept constant to keep the control on the threshold voltage. Using these optimizations, transistors with an average charge carrier mobility of 0.34 $cm^2V^{-1}s^{-1}$ are obtained. Reducing the gate dielectric and covering the gate oxide with phosphonic acid based SAMs leads to a subthreshold swing of $116\ mVdec^{-1}$ for undoped and $355\ mVdec^{-1}$ for highly doped transistors are obtained, albeit at a reduced charge carrier mobiliy.

## 5. Experimental Section

OFETs are assembled on glass substrates, which are cleaned by a sequence of ultrasonication in D.I. water, acetone, methanol and isopropanol, and drying in a stream of nitrogen. To assemble the dielectric gate, which includes gate oxide and passivation layer, an Aluminum film of 150 nm is deposited by thermal evaporation and structured by shadow masks to form gate patterns.

For TTC based OFETs (series #1 and #2), 50 nm of aluminum oxide (50 nm) is used as the dielectric gate material, which is grown by anodization according to the reports by Majewski et al..[52] The thickness of the aluminum oxide is controlled by the terminating voltage of anodization. Afterwards, substrates are annealed for 2 hr at a temperature of 70 °C. Finally, a passivation layer (40 nm film of TTC) is deposited onto the Aluminum oxide to complete the dielectric gate. Before the evaporation of organic semiconductors, substrates with dielectric gate are annealed again for another 2 hr at a temperature of 70 °C.

For SAMs based OFETs (series #3), Aluminum oxide is grown by oxygen plasma according to the reports by Klauk et al. [32] Afterwards, the samples are immersed in 5 mM solution of N-tetradecylphosphonic acid (TDPA) for 18hr to form a passivation layer of self-assembled monolayers (SAMs) on the oxide surface[32]. The samples are rinsed by Isopropanol and again dried by Nitrogen gas. Finally, samples are annealed for 20 min at 70 centigrade in a nitrogen filled glovebox.

The dopant film is deposited in a single evaporation run with different thickness at an evaporation rate of $0.1\ \text{Å}/s$. Afterwards, 40 nm of intrinsic $C_{60}$FHF film is thermally deposited at a rate of $0.5\ \text{Å}/s$.

The injection layer is deposited and patterned by a drain/ source shadow mask, followed by 60 nm of Aluminum film to ensure a high conductivity throughout the drain/ source electrodes. For OFETs with gold injection layer, 20 nm of gold is thermally deposited as the

injection layer. For OFETs with an n-type $C_{60}$ injection layer, the heavily doped $C_{60}$ film (25 nm, 8 wt.% of $C_{60}$: o-MeO-DMBI-I) is deposited by co-evaporation. During the co-evaporation, the doping concentration is controlled by the ratio of evapration rate between $C_{60}$ and the corresponding n-dopant o-MeO-DMBI-I. Here, the rate of $C_{60}$ is kept at $0.5\ Å/s$. Furthermore, a thin film of the pure n-dopant (2 nm, o-MeO-DMBI-I) is deposited on the top of n-type $C_{60}$ injection layer to further enhance the injection.

The vacuum chamber and deposition tool are manufactured by Angstrom Inc. The base pressure of the vacuum chamber is in the range of $5 \times 10^{-8}\ Torr$. The transistors are characterized by a Keithley SCS-4200 semiconductor parameter analyzer inside the glovebox at room temperature (300 K). The level of oxygen and moisture in the glovebox are controlled and remained below 0.1 ppm. The average value and standard deviation of 8 transistors per data point are plotted in Figure 6, Figure 7 and Figure 8.

Aluminum and gold are purchased from Sigma-Aldrich with a purity of 99.999%. The n-dopant o-MeO-DMBI-I are purchased from Lumtech with a purity of 99.9%. $C_{60}$ is purchased from Creaphys GmbH with a purity of 99.99%. All materials are used without further purification.

**Supporting Information**

Supporting Information is available from the Wiley Online Library or from the author.

Acknowledgements

The generous support of National Science Foundation (grant NSF-CHE-1362302 (to S.H.S. and O.V.B.; grant EECS 1709479 to B.L.) is acknowledged. Devices were prepared at the Prototype Facility of the Liquid Crystal Institute, Kent State University.

Received: ((will be filled in by the editorial staff))
Revised: ((will be filled in by the editorial staff))
Published online: ((will be filled in by the editorial staff))

References

[1] C. Rolin, E. Kang, J. H. Lee, G. Borghs, P. Heremans, J. Genoe, *Nat. Commun.* **2017**, *8*, 14975.

[2] Y. Yuan, G. Giri, A. L. Ayzner, A. P. Zoombelt, S. C. B. Mannsfeld, J. Chen, D. Nordlund, M. F. Toney, J. Huang, Z. Bao, *Nat. Commun.* **2014**, *5*, 3005.

[3] E. G. Bittle, J. I. Basham, T. N. Jackson, O. D. Jurchescu, D. J. Gundlach, *Nat. Commun.* **2016**, *7*, 10908.

[4] A. Perinot, P. Kshirsagar, M. A. Malvindi, P. P. Pompa, R. Fiammengo, M. Caironi, *Sci. Rep.* **2016**, *6*, 38941.

[5] M. Uno, B. S. Cha, Y. Kanaoka, J. Takeya, *Org. Electron.* **2015**, *20*, 119.

[6] M. Kitamura, Y. Arakawa, *Jpn. J. Appl. Phys.* **2011**, *50*, 01BC01.

[7] T. W. Canzler, U. Denker, O. Fadhel, Q. Huang, C. Rothe, A. Werner, in *Proc. SPIE 7054*, **2008**, p. 70540O.

[8] F. Ante, D. Kälblein, U. Zschieschang, T. W. Canzler, A. Werner, K. Takimiya, M. Ikeda, T. Sekitani, T. Someya, H. Klauk, D. Kaelblein, U. Zschieschang, T. W. Canzler, A. Werner, K. Takimiya, M. Ikeda, T. Sekitani, T. Someya, H. Klauk, *Small* **2011**, *7*, 1186.

[9] Y. Abe, T. Hasegawa, Y. Takahashi, T. Yamada, Y. Tokura, *Appl. Phys. Lett.* **2005**, *87*, 153506.

[10] E. Lim, B.-J. Jung, M. Chikamatsu, R. Azumi, Y. Yoshida, K. Yase, L.-M. Do, H.-K. Shim, *J. Mater. Chem.* **2007**, *17*, 1416.

[11] L. Ma, W. H. Lee, Y. D. Park, J. S. Kim, H. S. Lee, K. Choa, K. Cho, *Appl. Phys. Lett.* **2008**, *92*, 063310.

[12] B. Lüssem, M. L. M. L. Tietze, H. Kleemann, C. Hoßbach, J. W. J. W. Bartha, A. Zakhidov, K. Leo, *Nat. Commun.* **2013**, *4*, 2775.

[13] B. Lüssem, C.-M. C. Keum, D. Kasemann, B. Naab, Z. Bao, K. Leo, B. Lussem, C.-M. C. Keum, D. Kasemann, B. Naab, Z. Bao, K. Leo, *Chem. Rev.* **2016**, *116*, 13714.

[14] M. P. M. P. Hein, A. A. A. Zakhidov, B. Lüssem, J. Jankowski, M. L. M. L. Tietze, M. K. M. K. Riede, K. Leo, *Appl. Phys. Lett.* **2014**, *104*, 013507.

[15] P. Wei, J. H. Oh, G. Dong, Z. Bao, *J. Am. Chem. Soc.* **2010**, *132*, 8852.

[16] S. Liu, A. Al-Shadeedi, V. Kaphle, B. Lüssem, *SID Symp. Dig. Tech. Pap.* **2018**, *49*, 884.

[17] A. Al-Shadeedi, S. Liu, C. Keum, D. Kasemann, C. Hoßbach, J. Bartha, S. D. Bunge, *ACS Appl. Mater. Interfaces* **2016**, *8*, 32432.

[18] B. Lüssem, H. Kleemann, D. Kasemann, F. Ventsch, K. Leo, *Adv. Funct. Mater.* **2014**, *24*, 1011.

[19] Y. Zhao, Y. Guo, Y. Liu, *Adv. Mater.* **2013**, *25*, 5372.

[20] K. Walzer, B. Maennig, M. Pfeiffer, K. Leo, *Chem. Rev.* **2007**, *107*, 1233.

[21] R. C. Haddon, A. S. Perel, R. C. Morris, T. T. M. Palstra, A. F. Hebard, R. M. Fleming, *Appl. Phys. Lett.* **1995**, *67*, 121.

[22] S. Kobayashi, T. Takenobu, S. Mon, a. Fujiwara, Y. Iwasa, *Appl. Phys. Lett.* **2003**, *82*, 4581.

[23] H. Li, B. Tee, J. Cha, Y. Cui, J. Chung, S. Lee, Z. Bao, *J. Am. Chem. Soc.* **2012**, *134*, 2760.

[24] J. H. Oh, P. Wei, Z. Bao, *Appl. Phys. Lett.* **2010**, *97*, 243305.

[25] Y. Zhang, I. Murtaza, H. Meng, *J. Mater. Chem. C* **2018**, *6*, 3514.

[26] H. Yu, H. H. Cho, C. H. Cho, K. H. Kim, D. Y. Kim, B. J. Kim, J. H. Oh, *ACS Appl. Mater. Interfaces* **2013**, *5*, 4865.

[27] B. W. Larson, J. B. Whitaker, A. A. Popov, N. Kopidakis, G. Rumbles, O. V. Boltalina, S. H. Strauss, *Chem. Mater.* **2014**, *26*, 2361.

[28] S. Liu, Y.-J. Lu, M. M. Kappes, J. A. Ibers, *Science (80-. ).* **1991**, *254*, 408.

[29] L. K. San, E. V. Bukovsky, B. W. Larson, J. B. Whitaker, S. H. M. Deng, N. Kopidakis, G. Rumbles, A. A. Popov, Y. S. Chen, X. Bin Wang, O. V. Boltalina, S. H.

Strauss, *Chem. Sci.* **2015**, *6*, 1801.

[30] G. Paternò, A. J. Warren, J. Spencer, G. Evans, V. G. Sakai, J. Blumberger, F. Cacialli, *J. Mater. Chem. C* **2013**, *1*, 5619.

[31] R. J. Baker, P. E. Colavita, D. M. Murphy, J. A. Platts, J. D. Wallis, *J. Phys. Chem. A* **2012**, *116*, 1435.

[32] H. Omorodion, B. Twamley, J. A. Platts, R. J. Baker, *Cryst. Growth Des.* **2015**, *15*, 2835.

[33] X. Liu, C. D. Mcmillen, J. S. Thrasher, *New J. Chem.* **2018**, *42*, 10484.

[34] M. Kraus, S. Richler, A. Opitz, W. Brütting, S. Haas, T. Hasegawa, A. Hinderhofer, F. Schreiber, *J. Appl. Phys.* **2010**, *107*, DOI 10.1063/1.3354086.

[35] H. Klauk, U. Zschieschang, J. Pflaum, M. Halik, *Nature* **2007**, *445*, 745.

[36] J. Blochwitz, T. Fritz, M. Pfeiffer, K. Leo, D. M. Alloway, P. A. Lee, N. R. Armstrong, *Org. Electron.* **2001**, *2*, 97.

[37] S. Ogawa, Y. Kimura, M. Niwano, H. Ishii, *Appl. Phys. Lett.* **2007**, *90*, 1.

[38] U. Zschieschang, R. T. Weitz, K. Kern, H. Klauk, *Appl. Phys. A Mater. Sci. Process.* **2009**, *95*, 139.

[39] C. Liu, Y. Xu, Y. Y. Noh, *Mater. Today* **2015**, *18*, 79.

[40] H. Klauk, *Adv. Electron. Mater.* **2018**, *10*, 1700474.

[41] H. Kleemann, A. A. A. Zakhidov, M. Anderson, T. Menke, K. Leo, B. Lüssem, *Org. Electron.* **2012**, *13*, 506.

[42] S. Singh, S. K. Mohapatra, A. Sharma, C. Fuentes-Hernandez, S. Barlow, S. R. Marder, B. Kippelen, *Appl. Phys. Lett.* **2013**, *102*, 153303.

[43] T. Hähnlen, C. Vanoni, C. Wäckerlin, T. a. Jung, S. Tsujino, *Appl. Phys. Lett.* **2012**, *101*, 033305.

[44] S. Olthof, S. Singh, S. K. Mohapatra, S. Barlow, S. R. Marder, B. Kippelen, A. Kahn, *Appl. Phys. Lett.* **2012**, *101*, 253303.

[45] G. Horowitz, R. Hajlaoui, H. Bouchriha, R. Bourguiga, M. Hajlaoui, *Adv. Mater.* **1998**, *10*, 923.

[46] W. Zhao, Y. Qi, T. Sajoto, S. Barlow, S. R. Marder, A. Kahn, *Appl. Phys. Lett.* **2010**, *97*, 1.

[47] S. J. Ausserlechner, M. Gruber, R. Hetzel, H. G. Flesch, L. Ladinig, L. Hauser, A. Haase, M. Buchner, R. Resel, F. Schürrer, B. Stadlober, G. Trimmel, K. Zojer, E. Zojer, *Phys. Status Solidi Appl. Mater. Sci.* **2012**, *209*, 181.

[48] M. Marchl, M. Edler, A. Haase, A. Fian, G. Trimmel, T. Griesser, B. Stadlober, E. Zojer, *Adv. Mater.* **2010**, *22*, 5361.

[49] H. Kleemann, C. Schuenemann, A. A. A. Zakhidov, M. Riede, B. Lüssem, K. Leo, *Org. Electron.* **2012**, *13*, 58.

[50] H. Kleemann, B. Lüssem, K. Leo, *J. Appl. Phys.* **2012**, *111*, 123722.

[51] S. Liu, A. Al-Shadeedi, C.-M. Keum, B. Lussem, *Nanotechnology* **2018**, *29*, 284001.

[52] L. A. Majewski, R. Schroeder, M. Voigt, M. Grell, *J. Phys. D. Appl. Phys.* **2004**, *37*, 3367.

[53] E. J. Meijer, C. Detcheverry, P. J. Baesjou, E. van Veenendaal, D. M. de Leeuw, T. M. Klapwijk, *J. Appl. Phys.* **2003**, *93*, 4831.

**The table of contents entry should be 50–60 words long**, and the first phrase should be bold.

Faux-hawk fullerenes combine high thermal stability with high packing density and a lowest unoccupied molecular orbital position favorable for organic field-effect transistors (OFETs). Based on an improved synthetic procedure, the performance of faux hawk fullerene based n-doped OFETs is studied. An analytical model describing the influence of doping on n-type OFETs is presented, which is used to optimize transistors, resulting in a high electron mobility (0.34), low subthreshold swing ($355\ mVdec^{-1}$) and low contact resistances.

**Keyword**
$C_{60}$, Faux Hawk Fullerene, Organic Field-Effect Transistor, Doping, Transfer Doping

*Shiyi Liu, Nicholas J. DeWeerd, Brian J. Reeves, Long K. San, Steven H. Strauss, Olga V. Boltalina, Björn Lüssem**

S. Liu, Assoc. Prof. B. Lüssem
Department of Physics
Kent State University
Kent, OH, 44240
E-mail: blussem@kent.edu

N. J. DeWeerd, B. J. Reeves, Dr. L. K. San, Prof. S. H. Strauss, Dr. O. V. Boltalina
Department of Chemistry
Colorado State University
Fort Collins, CO 80523, USA.
E-mail: olga.boltalina@colostate.edu

**Doped n-type Organic Field-Effect Transistors based on Faux Hawk Fullerene**

ToC figure ((Please choose one size: 55 mm broad × 50 mm high **or** 110 mm broad × 20 mm high. Please do not use any other dimensions))

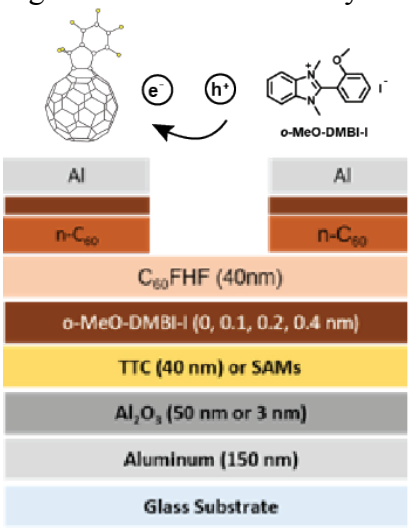

# Supporting Information

## Doped n-type Organic Field-Effect Transistors based on Faux Hawk Fullerene

*Shiyi Liu, Nicholas J. DeWeerd, Brian J. Reeves, Long K. San, Steven H. Strauss, Olga V. Boltalina, Björn Lüssem**

S. Liu, Assoc. Prof. B. Lüssem
Department of Physics
Kent State University
Kent, OH, 44240
E-mail: blussem@kent.edu

N. J. DeWeerd, B. J. Reeves, L. K. San, S. H. Strauss, Dr. O. V. Boltalina
Department of Chemistry
Colorado State University
Fort Collins, CO 80523, USA.
E-mail: olga.boltalina@colostate.edu

### 1. Synthesis of $C_{60}FHF$ using large scale optimized conditions

$C_{60}$, 200 mg (0.2 mmol), was added to a clean and flame dried Schlenk flask, under a flush of nitrogen. The flask was then sealed under a positive pressure of nitrogen and opened again in a UHP nitrogen, glovebox. Anhydrous *o*-dichlorobenzene, (35 mL, resulting fullerene concentration 6.0 mM), was added along with a stir bar and 1.1 equivalents of tributyl tin hydride (82 µL). Also at this time anhydrous pyridine, 10% by volume, (3.5 mL) was added to the crude solution. The reaction flask was then sealed and sonicated for approx. 15 minutes or until all $C_{60}$ was dissolved. Afterwards, under a flush of nitrogen 1.1 equivalents of perfluorobenzyl iodide (48 µL) was added via a glass syringe. The flask was then resealed under a positive pressure and all remaining gasses were removed from both the solution and the head space of the flask via the freeze-pump-thaw method. After 3 freeze-pump-thaw cycles, and the degassed solution had warmed to approx. room temperature, the reaction flask was placed in a 145 °C oil bath with stirring for 16 h. After the reaction period the solution

had changed from a dark purple to brown. The resulting solution was then transferred to a round bottom flask in air and roto-evaporated to near dryness. The dark brown sludge was washed with heptane, sonicated, and then roto-evaporated to azeotrope any remaining *o*-dichlorobenzene. This procedure was repeated 3 times. The resulting brown powder was dissolved in toluene and was then separated by HPLC on a Cosmosil Buckyprep column with a flow rate of 5 mL $min^{-1}$. These reactions were repeated at this scale several times in order to synthesize the 100 mg amount required for the analyses.

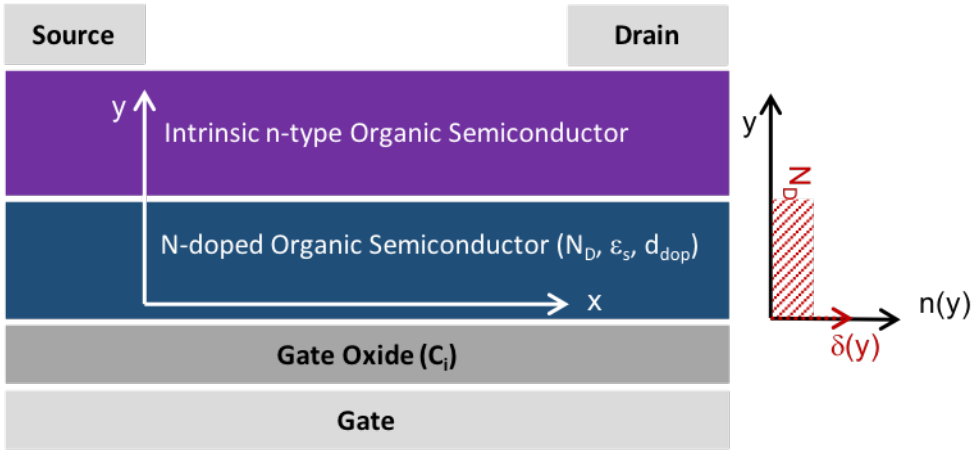


**Figure S1:** General setup of an n-doped Organic Field-Effect Transistor

## 2. Drain Current of n-doped OFETs operated in Saturation

An expression for the drain current of n-doped OFETs is derived analogous to the case of p-doped OFETs discussed previously.[16] A simplified device structure as shown in Figure S1 is assumed. Here, $x$ denotes the position inside the channel. The edge of the source contact is set to $x = 0$.

The total density of electrons inside the channel becomes:

$$n = \frac{1}{e} C_i \left(V_{GS} - V_{FB} - V(x)\right)\delta(y) + N_D(y) \qquad \text{(Eq. S1)}$$

with $e$: elementary charge, $V_{GS}$: gate potential, $V_{FB}$: flatband voltage of the MOS capacitor, $V(x)$: electric potential inside the channel, $C_i$ the specific gate capacitance, and and $\delta(y)$ the Dirac Delta function.

Assuming a thin and homogeneous doped layer at the gate dielectric/organic semiconductor interface with thickness $d_{dop}$, the doping profile $N_D(y)$ becomes:

$$N_D(y) = \begin{cases} N_D\,; & \text{for } 0 \le y \le d_{dop} \\ 0; & y > d_{dop} \end{cases} \quad \text{(Eq. S2)}$$

In the linear regime, the drain current $I_D$ becomes

$$-I_D = we\int_0^\infty n(y)\mu E_x dy = w\mu\left(-\frac{dV(x)}{dx}\right)C_i\left\{(V_{GS} - V_{FB} - V(x)) + \frac{N_D d_{dop} e}{C_i}\right\} \quad \text{(Eq. S3)}$$

with $w$: channel width, $\mu$: electron mobility, $E_x = -\frac{dV(x)}{dx}$: x-component of the electric field.

Integrating Eq. S3 along the transistor channel (channel lenght $L$) leads to

$$\int_0^L I_D = w\mu C_i \int_0^{V_{DS}} \left\{(V_{GS} - V_{FB} - V(x)) + \frac{N_D d_{dop} e}{C_i}\right\} dV \quad \text{(Eq. S4)}$$

$$I_D = k\left\{(V_{GS} - V_{th})V_{DS} - \frac{V_{DS}^2}{2}\right\} \quad \text{(Eq. S5)}$$

Where $k = \frac{w\mu C_i}{L}$, $V_{DS}$ is the drain potential, and $V_{th}$ the threshold voltage, which becomes $V_{th} = V_{FB} - \frac{eN_D d_{dop}}{C_i}$. Eq. S5 is valid in the linear regime only. As for intrinsic transistors, one can approximate Eq. S5 with $I_D = k(V_{GS} - V_{th})V_{DS}$ if $V_{GS} - V_{FB} > V_{DS}$.

In the saturation regime, i.e. for $V_{DS} > V_{GS} - V_{FB}$, the influence of the depletion of the doped layer at the drain electrode has to be taken into account and one has to adapt Eq. S4 [45]

$$I_D = k\int_0^{V_{GS}-V_{FB}} V_{GS} - V_{th} - V(x)dV + \frac{k}{C_i} eN_D \int_{V_{GS}-V_{FB}}^{V_{D,sat}} \left(d_{dop} - d_{dep}\right) dV \quad \text{(Eq. S7)}$$

With $d_{dep}$ the thickness of the depletion inside the channel, which can be expressed as ($\varepsilon_S$: permittivity of the organic layer)[53]

$$d_{dep} = \frac{\varepsilon_S}{C_i}\left\{\sqrt{1 + \frac{2C_i^2(V(x) - V_{GS} + V_{FB})}{eN_D\varepsilon_S}} - 1\right\} \quad \text{(Eq. S8)}$$

With the help of Eq. S8, the second integral of Eq. S7 can be re-written as an integral with respect to the depletion layer thickness:

$$\frac{k}{C_i} eN_D \int_{V_{GS}-V_{FB}}^{V_{D,sat}} \left(d_{dop} - d_{dep}\right) dV = \frac{ke^2 N_D^2}{\varepsilon_S C_i} \int_0^{d_{dep}(x=L)} \left(d_{dop} - d_{dep}\right) \left\{d_{dep} + \frac{\varepsilon_S}{C_i}\right\} dd_{dop} \quad \text{(Eq. S9)}$$

For saturation, the depletion layer thickness at the drain $d_{dep}(x = L)$ equals the complete doped layer thickness, i.e. $d_{dep}(x = L) = d_{dop}$. Solving the integrals in Eqs. S7 and S9 finally leads to the following saturation current $I_{D,sat}$:

$$I_{D,sat} = \frac{\mu_n w C_i}{2L} \left[(V_{GS} - V_{th})^2 - \frac{2}{3} \frac{e d_{dop} N_D}{C_i} \cdot (V_{PO} - V_{th})\right] \quad \text{(Eq. S10)}$$

Here, the pinch-off voltage $V_{PO}$ is defined as the gate voltage $V_{GS}$ that has to be applied to fully deplete the channel from doped charges. Depletion is latest at the source electrode. Setting $V_{GS} = V_{PO}$ and $V(x = 0) = 0$ (i.e. the potential at the source is 0 V) in Eq. S8 leads to

$$V_{PO} = V_{th} - \frac{eN_D d_{dop}}{2C_s} \quad \text{(Eq. S11)}$$